

Diffusion limited mixing in confined media

Mayumi Hamada,¹ Luis Cueto-Felgueroso,² and Pietro de Anna^{1,*}

¹*Institute of Earth Science, University of Lausanne, 1015 Lausanne, Switzerland*

²*Department of Civil Engineering: Hydraulics, Energy and the Environment, Technical University of Madrid (UPM), 28040 Madrid, Spain*



(Received 20 May 2020; accepted 24 November 2020;
published 18 December 2020)

Diffusion controls a plethora of natural and industrial phenomena. Directly, as in intracellular transport and gas exchange in the lungs, or indirectly, in processes that are driven by the encounter of different entities through their mixing: e.g., microbes and nutrients or species involved in chemical reactions. When mixing happens in confined environments that are characterized by the presence of impermeable boundaries, the species spatial organization deviates from the one observed in unconfined systems. Here, we investigate the impact of confinement on mixing state and rate. We use the analytical solution of a one-dimensional diffusion equation for a finite spatial domain of size λ to quantify the impact of confinement on several mixing measures, such as the concentration and gradients probability density function, scalar dissipation rate, and dilution index. We show that no-flux boundary conditions lead to a new timescale characterizing confinement-limited mixing controlled by diffusion, $\lambda^2/(D\pi^2)$, which is significantly shorter (one order of magnitude shorter) than the characteristic diffusive timescale, λ^2/D , in an unconfined domain. These observations show that the diffusive homogenization mechanism is enhanced by the presence of impermeable boundaries and, thus, mixing happens much faster under confinement.

DOI: [10.1103/PhysRevFluids.5.124502](https://doi.org/10.1103/PhysRevFluids.5.124502)

I. INTRODUCTION

In both natural and industrial systems, and across scales, the ability of dissolved compounds to react is controlled by the efficiency of the system to mix them, promoting their physical encounter. In a quiescent fluid the mixing process is driven by the sole action of diffusion. In the presence of advection (e.g., a stirred mixture or a flowing solute) the mixing front stretches, due to heterogeneity in flow velocities, while it diffuses, leading to the complex competition between these two effects, the first increasing and the second reducing solute concentration gradients [1,2]. This combined action results in a mixing mechanism by which initially segregated substances are led to occupy the same volume [3,4]. Classical mixing measures, such as the scalar dissipation rate [5], the degree of mixing [6], or the dilution index [7,8] (a measure of the system entropy), are based on the detailed knowledge of the spatial distribution of the solute concentrations and their gradients.

*pietro.deanna@unil.ch

Published by the American Physical Society under the terms of the [Creative Commons Attribution 4.0 International](https://creativecommons.org/licenses/by/4.0/) license. Further distribution of this work must maintain attribution to the author(s) and the published article's title, journal citation, and DOI.

A mass conservation equation controls the spatiotemporal distribution of a passive tracer concentration, c , through the well-known advection-diffusion equation [2,9]:

$$\frac{\partial c}{\partial t} = -\mathbf{u} \cdot \nabla c + D\nabla^2 c, \quad (1)$$

where D is the diffusion coefficient and \mathbf{u} is the velocity field experienced by the tracer. Solving Eq. (1) across several temporal and spatial scales is necessary to understand important scientific questions (e.g., kinetics of reactions or microbial growth) and to address industrial (e.g., bioremediation, filtration) and societal issues (e.g., efficient design of water treatment solutions). In most practical applications, it is challenging to solve Eq. (1) via numerical simulation or measuring c across relevant spatial/temporal scales. Thus, upscaling techniques that focus on the controlling physical mechanisms to predict their larger scale impact have been developed, including volume averaging methods [10] or statistical models, such as the continuous time random walk [11], multirate-mass-transfer [11], or the lamellar framework [8]. The latter has been successfully applied to a wide range of flow systems characterized with a different flow kinematics, as turbulent [12], chaotic [4], or laminar flows [8,13,14].

In a lamellar framework, a transported scalar field is characterized by a displacing front organized as an ensemble of thin and elongated structures, called lamellae, which are stretched and folded by the background heterogeneous flow field and typically characterized by their length $l(t)$ and width $s(t)$ [15]. An individual lamella undergoes the following geometrical changes, as it is moved: (i) it is displaced and stretched by the flow kinematics, (ii) it diffuses along the front transverse direction, and (iii) it eventually merges with another lamella to form larger lamella bundles [4,8,15]. The model then solves Eq. (1) for a single lamella in a Lagrangian framework:

$$\frac{\partial c}{\partial t} = -\frac{n}{s} \frac{ds}{dt} \frac{\partial c}{\partial n} + D \frac{\partial^2 c}{\partial n^2}, \quad (2)$$

where n denotes the spatial coordinate in the direction perpendicular to the lamella, along which diffusion takes place. Using the Ranz transform [15,16], space is normalized by the lamella width $s(t)$, $\bar{n} = n/s(t)$ and time is expressed in terms of diffusion time $s(t)^2/D$, $\bar{t} = D \int_0^t 1/s(t')^2 dt'$. Thus, mixing reduces to a one-dimensional diffusion problem:

$$\frac{\partial c}{\partial \bar{t}} = \frac{\partial^2 c}{\partial \bar{n}^2}. \quad (3)$$

The mixing driven by these processes is then modeled considering the dynamics of the average between several lamellae thicknesses that individually takes place only along the direction transverse to the local front. This diffusion equation controls mixing-driven phenomena also in many other situations where a mixing front is steady (as in microreactors where solutes are injected side-by-side) and the kinematics of fluid motion can be neglected. For continuous systems where a tracer can freely diffuse across space, an initial pulse or front of tracer would result in a diffusive profile with Gaussian- or error function-like shape. However, several mixing-driven processes happen in media characterized by confinement, such as capillary tubes, batch reactors, or porous systems (as filters or soils): in such scenarios the walls defining the confined domain, e.g., a capillary tube surface or porous media grains, are considered impermeable. As a consequence, solutes within such confined systems cannot diffuse freely, as they will experience the impermeable walls where no-flux boundary conditions must be honored.

The goal of the present work is to describe the impact on mixing of the spatial distribution and temporal evolution of a diffusive tracer in a quiescent fluid (no flow) within a system characterized by confinement, such as reactors [15], porous or fractured media [13], and microfluidics [17,18]. To do so we solve the one-dimensional diffusion equation with no-flux boundary conditions and we assess the impact of the presence of boundaries on the following classical mixing measures: the scalar dissipation rate $\epsilon(t)$, the concentration c and gradient ∇c (whose value we denote by g_c), their corresponding probability density functions (PDFs), $p_c(c)$ and $p_g(g_c)$, and the dilution

index $E(t)$. Their results are all quantitatively and qualitatively different from the unconfined case. Our results represent the building block of mixing models for more complex systems involving distributed confinement size and fluid velocity heterogeneity.

II. RESULTS

We study a one-dimensional system in which a tracer undergoes molecular diffusion, for two initial configurations: at $t = 0$ the tracer is distributed either as a front or a pulse. These two initial conditions are paradigmatic cases of interest since many, more complex, configurations can be interpreted as a properly weighted statistical superposition of them. Furthermore, we consider two scenarios: (i) the system has infinite size, $x \in (-\infty, +\infty)$, also called an unconfined case and (ii) the system has finite size, $x \in [0, \lambda]$, also called a confined case. We introduce the following normalized space, time, and concentration:

$$\hat{x} = \frac{x}{\lambda}, \quad \hat{t} = \frac{t}{\tau_D}, \quad \hat{c} = \frac{c}{c_0}, \quad (4)$$

where λ is the characteristic confinement length scale, $\tau_D = \frac{\lambda^2}{D}$ is the characteristic time for diffusion, and c_0 is the maximum solute concentration at $t = 0$. Dropping hats for simplicity of notation, the spatiotemporal concentration distribution of a passive solute undergoing molecular diffusion is described by Fick's first law [19], stating that the mass flux is locally proportional to the concentration gradient and mass conservation, which together lead to the diffusion equation, here expressed in terms of dimensionless quantities:

$$\frac{\partial c}{\partial t} = \frac{\partial^2 c}{\partial x^2}. \quad (5)$$

In addition to metrics involving explicitly the spatial extent of the diffusing tracer, a way to quantify and characterize the system mixing is in terms of the tracer concentration distribution, or PDF. We introduce it in terms of $p_c(c, t)dc$, the probability of sampling a concentration value between c and $c + dc$ when the spatial domain is sampled uniformly, as equal to the probability $p_x(x, t)dx$ to find a given location between x and $x + dx$ when sampling mass uniformly. We derive $p_c(c, t)$ by inverting, when possible, and differentiating the spatial dependence of the scalar profile $c(x, t)$ obtaining

$$p_c(c, t)dc = p_x(x, t)dx, \quad \text{thus} \quad p_c(c, t) = p_x(x, t) \left| \frac{\partial x(c, t)}{\partial c} \right|. \quad (6)$$

In the configurations considered here, the profiles are invertible either on the full domain or on half of it. In that case they are also symmetrical and, thus, the PDF on half of the domain is equal to the one for the whole. The total probability of inspecting a point at any location with uniformly random sampling $p_x(x, t) = p(t)$ within the considered domain V is $P = \int_V p(t)dx = 1$ by definition, thus $p = 1/V$. However, in an unconfined domain with infinite size this probability is identically zero. Therefore, for an unconfined domain, we must consider a portion of it $x \in]-N, N[$ or $x \in]0, N[$, with arbitrarily large, but finite, N so that outside this domain the concentration is too small to be detected, $c < c_m$, where c_m represents the smallest concentration that is distinguishable from zero. In general, the size N of such domain must be time dependent, $N = N(t)$, since the concentration is spreading. For a profile invertible on the full domain we consider $x \in]-N, N[$ and thus

$$P[-N(t) < x < N(t)] = \int_{-N(t)}^{N(t)} p(t)dx = p(t)2N(t) = 1, \quad p = \frac{1}{2N(t)}; \quad (7)$$

if the profile is invertible only on half of the domain we have $x \in]-N, 0[$ and

$$P[-N(t) < x < 0] = \int_{-N(t)}^0 p(t)dx = p(t)N(t) = 1, \quad p = \frac{1}{N(t)}. \quad (8)$$

In the following we are going to solve the dimensionless diffusion equation (5), and compute different mixing measures and their scaling laws for an initial front/pulse for unconfined and confined scenarios.

A. Unconfined case

For an unconfined domain, $x \in (-\infty, +\infty)$, the partial differential equation (5) can be solved considering the Fourier transform along the spatial variable x , reducing Eq. (5) to an ordinary differential equation in the Fourier space, that can be solved and antitransformed. The well-known general solution of Eq. (5) is given by

$$c(x, t) = \frac{1}{\sqrt{4\pi t}} \int_{-\infty}^{+\infty} f_0(y) e^{-[(x-y)^2/4t]} dy, \quad (9)$$

where $f_0(x) = c(x, t = 0)$ is the initial concentration profile.

1. Initial concentration front

Assuming that the mass is initially distributed as a sharp front located at $x = 1/2$, we represent the initial condition as $f_0(x) = \theta(x - 1/2)$ [shown as a black solid line in Fig. 1(a)], invoking the Heaviside step function θ . Thus, the solution of (9) for this initial condition is

$$c(x, t) = \frac{1}{2} \left[1 - \operatorname{erf} \left(\frac{x - 1/2}{\sqrt{4t}} \right) \right], \quad (10)$$

which is shown, at different times ($t = 0.0045, 0.016, 0.12, \text{ and } 0.43$, from light to dark), in Fig. 1(a) as pink solid lines. As time passes, the initially sharp concentration profile evolves towards a smoother profile, spreading across the unconfined domain.

The spatial distribution of concentration $c(x, t)$ can be mapped into its PDF $p(c)$, as defined by Eq. (6). We denote by $N(t)$ the distance from $x = 1/2$ to the location where concentration attains the smallest detectable value c_m , $c(x = -N, t) = c_m$ and, by symmetry, it is also the distance from $x = 1/2$ where concentration is higher than $1 - c_m$, $c(x = N, t) = 1 - c_m$. Thus, the normalization of the PDF is $p(t) = 1/[2N(t)]$ and

$$N(t) = \sqrt{4t} \operatorname{erf}^{-1}(2c_m - 1), \quad \text{therefore} \quad p(t) = -\frac{1}{4\sqrt{t} \operatorname{erf}^{-1}(2c_m - 1)}. \quad (11)$$

Note that $\operatorname{erf}^{-1}(2c_m - 1)$ is negative, ensuring that p is positive. Finally, using Eq. (11), inverting and differentiating Eq. (10) we get

$$p_c(c) = -\frac{\sqrt{\pi}}{2 \operatorname{erf}^{-1}(2c_m - 1)} e^{[\operatorname{erf}^{-1}(2c_m - 1)]^2}. \quad (12)$$

We observe that under unconfined conditions a diffusive solute of concentration c has a PDF which is independent of time. This is also shown in Fig. 2(a) where $p_c(c)$ is plotted as solid pink lines, with color ranging from light to dark with increasing time (all solutions collapse on a single curve).

The degree of mixing reached by the diffusing system at a given time can be measured in terms of the system entropy or dilution index [7], defined as

$$E(t) = \exp \left(- \int c(x, t) \ln[c(x, t)] dx \right). \quad (13)$$

Inserting Eq. (10) into the previous expression we obtain

$$E(t) = \exp(\sqrt{2t} I), \quad \text{where} \quad I = - \int_{-\infty}^{\infty} \frac{1}{2} [1 + \operatorname{erf}(y)] \ln \left(\frac{1}{2} [1 + \operatorname{erf}(y)] \right) dy, \quad (14)$$

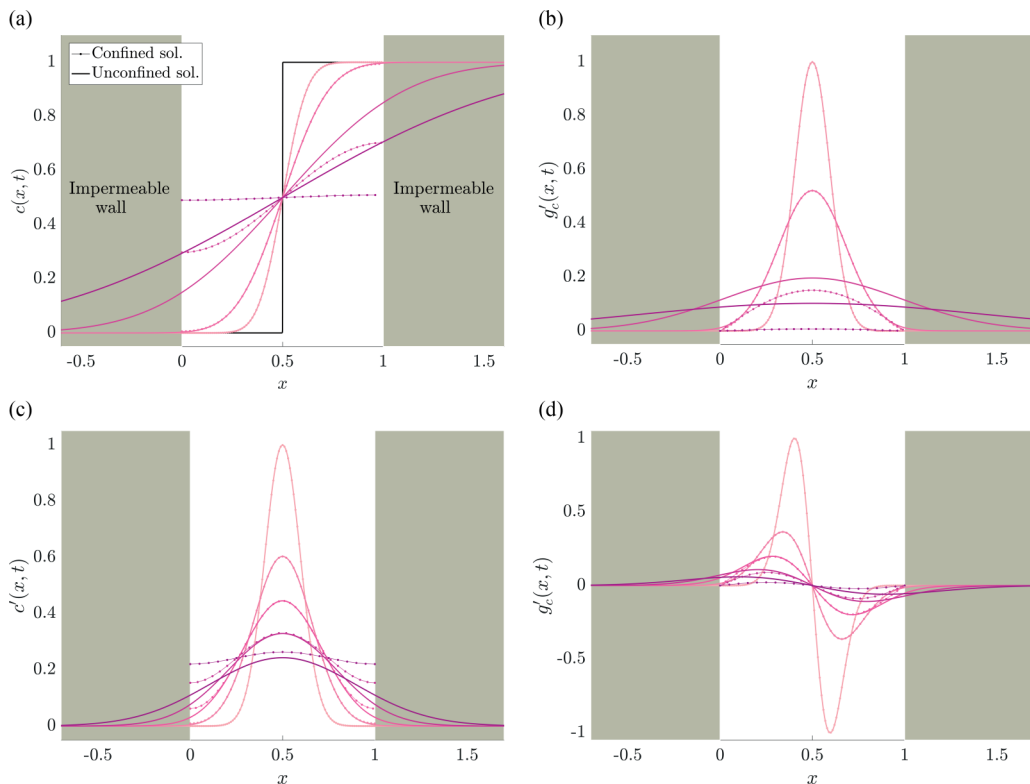


FIG. 1. Profile of concentration c and its gradient ∇c predicted by the analytical solution of a one-dimensional diffusion equation in an unconfined [Eq. (9) (solid line)] and confined [Eq. (31) (dotted line)] domain. (a) Concentration profile for a front concentration initial condition (black line), in unconfined Eq. (10) and confined Eq. (31) domains. (b) Concentration gradient normalized by its maximum value at time $t = 0.0045$ for the profiles in (a): each line in both plots corresponds to the normalized time $t = 0.0045, 0.016, 0.12, \text{ and } 0.43$. (c) Concentration profile for a pulse initial condition in unconfined domain, Eq. (18), normalized by its maximum value at time $t = 0.0047$ and confined domain, Eq. (31). (d) Concentration gradient for the profiles in (c): each line corresponds to a different normalized time $t = 0.0047, 0.013, 0.023, 0.043, \text{ and } 0.079$.

having introduced the coordinate $y = \frac{x}{\sqrt{2Dt}}$. The previous exact analytical expression is shown in Fig. 3(a) in a double-logarithmic plot versus time and in Fig. 3(b) as a semilogarithmic plot versus \sqrt{t} , as pink dots: from its initial value $E(0) = 1$ (note that at $t = 0$ the concentration has value either 0 or 1) it keeps increasing as $e^{\sqrt{t}}$ for all times as result of the infinite space where the concentration can mix (and dilute) indefinitely.

The spatial variability of the concentration solution, Eq. (10), is quantified by its gradient, i.e., its spatial derivative, that is,

$$\nabla c = \frac{1}{\sqrt{4\pi t}} e^{-[(x-1/2)^2/4t]}. \quad (15)$$

The previous expression is shown in Fig. 1(b) as a solid pink line ranging from light to dark as time increases with the same steps of the associated concentration profile ($t = 0.0045, 0.016, 0.12, \text{ and } 0.43$). Since the previous expression also represents the spatial distribution of a diffusing pulse, its PDF is discussed in the next section.

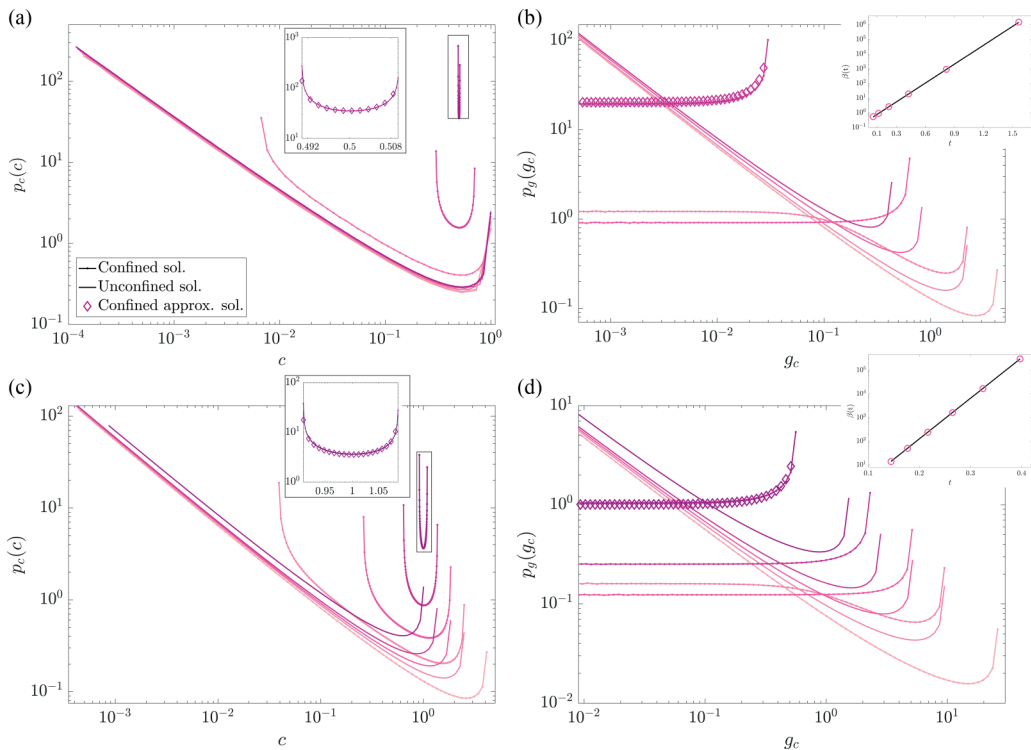


FIG. 2. Probability density function (PDF) p_c and p_g of concentration c and gradient g_c values, shown in Fig. 1, for confined (solid line) and unconfined (solid-dotted line) cases: each line corresponds to the same rescaled times as in Fig. 1: color scale goes from light to dark as time increases. (a) and (b) are concentration and gradient PDFs for a front initial condition while (c) and (d) are concentration and gradient PDFs for an initial pulse. Diamonds represent the approximated solutions derived for the confined cases. The insets in (a) and (c) are zoomed-in views of the PDF for the last time step. Insets of (b) and (d) represent the temporal evolution of the plateau value β .

As time passes the gradient maximum value g_M reached at $x = 1/2$ decreases as $g_M = 1/\sqrt{4\pi t}$ [as shown in Fig. 4(a) in a semilogarithmic plot and in Fig. 4(b) in a double-logarithmic plot], while it broadens as measured by the square root of its variance, that scales as $\sqrt{2t}$. The rate at which the considered diffusive system is mixing is then quantified by the scalar dissipation rate as

$$\epsilon(t) = \int_{-\infty}^{+\infty} \nabla c^T \nabla c dx, \quad (16)$$

which quantifies the spatial availability of concentration gradients that allows the Fickian mass flux to take place. It is a measure of mixing because it is related to the time derivative of the square of concentration [6] and therefore is related to a measure of the concentration fluctuations. In the case where the considered system is finite, boundary terms appear; however, if no-flux boundary conditions apply ($\nabla c|_S = 0$), these boundary terms are identically zero and play no role at all times. Defining the change of variable $y = (x - 1/2)/\sqrt{4t}$, we obtain

$$\epsilon(t) = \frac{1}{\sqrt{4\pi^2 t}} \int_{-\infty}^{+\infty} e^{-2y^2} dy = \frac{1}{\sqrt{8\pi t}}, \quad (17)$$

as shown in Figs. 4(c) and 4(d), where it is displayed through a semilogarithmic and double-logarithmic plot, respectively. The scaling of the scalar dissipation rate reflects that of the average

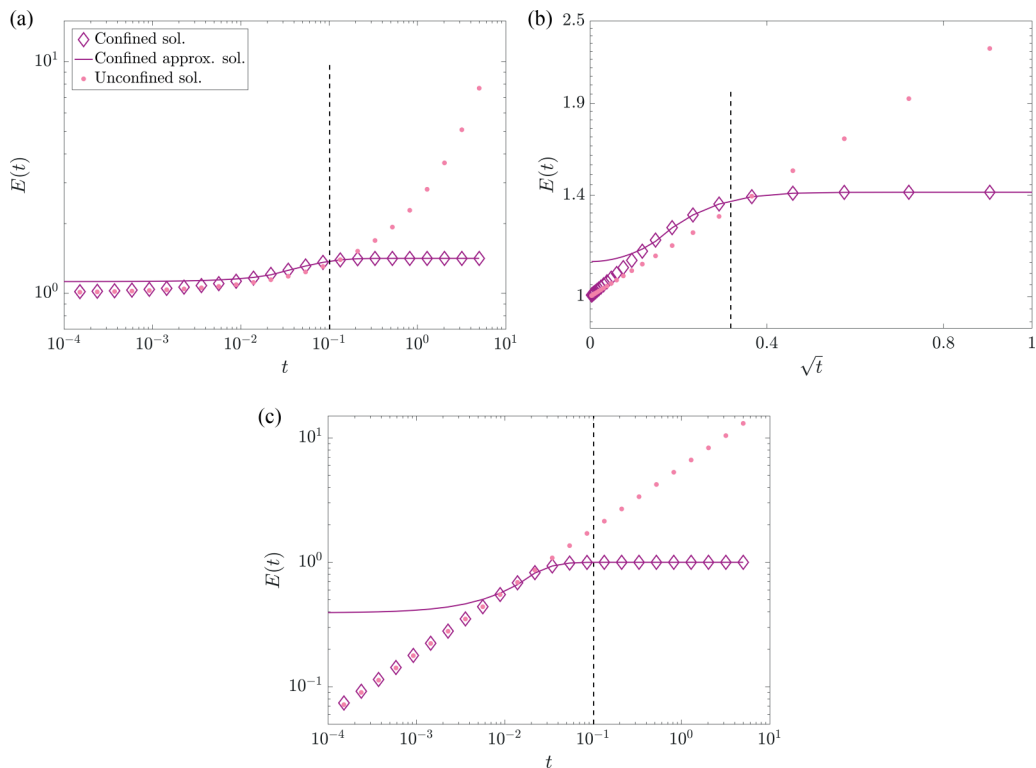


FIG. 3. Temporal evolution of the dilution index $E(t)$, Eq. (13). (a) and (b) show the front initial condition: in (b) the semilogarithmic representation of E versus \sqrt{t} emphasizes the scaling $e^{\sqrt{t}}$ for early times. (c) Pulse initial condition. For all initial conditions, the unconfined case (pink dots) grows indefinitely, while the confined case (diamonds) reaches its maximum value (complete mixing) earlier than $t = 1/\pi^2$ (vertical dashed black line). The solid line represents the approximated analytical solution computed.

gradient that can be approximated by the ratio of $g_M \approx t^{-1/2}$ and its spreading rate $t^{1/2}$, so that $\frac{g}{\sqrt{c}} \sim t^{-1/4}$.

2. Initial concentration pulse

If we consider the paradigmatic case of a pulse initial condition, for which all the mass is initially located at $x = 1/2$, as described by $f_0(x) = \delta(x - 1/2)$, the concentration profile is the well-known Gaussian function

$$c(x, t) = \frac{1}{\sqrt{4\pi t}} e^{-[(x-1/2)^2/4t]}, \quad c_M = c(x = 1/2) = \frac{1}{\sqrt{4\pi t}}, \quad (18)$$

which is characterized by the decay of its maximum value c_M and its lateral spreading. In Fig. 1 $c'(x, t) = c(x, t)/c(x, t_0)$, where $t_0 = 0.0047$, it is shown at four times steps ($t = 0.0047, 0.0128, 0.0234, 0.043$, and 0.0788), as a pink solid line ranging from light to dark as time increases. We notice that the concentration profile for a pulse initial condition, Eq. (18), is exactly the gradient of the concentration profile of a front: this is a consequence of the linearity of the diffusion equation and the fact that an initial pulse corresponds to the gradient of an initial front. Below we show that it is not the case in a confined domain.

The PDF of this profile can be derived from Eq. (6). The profile is invertible only on half of the domain $x \in]0, N[$ so $p = 1/N$, computing N as described above, inverting and differentiating

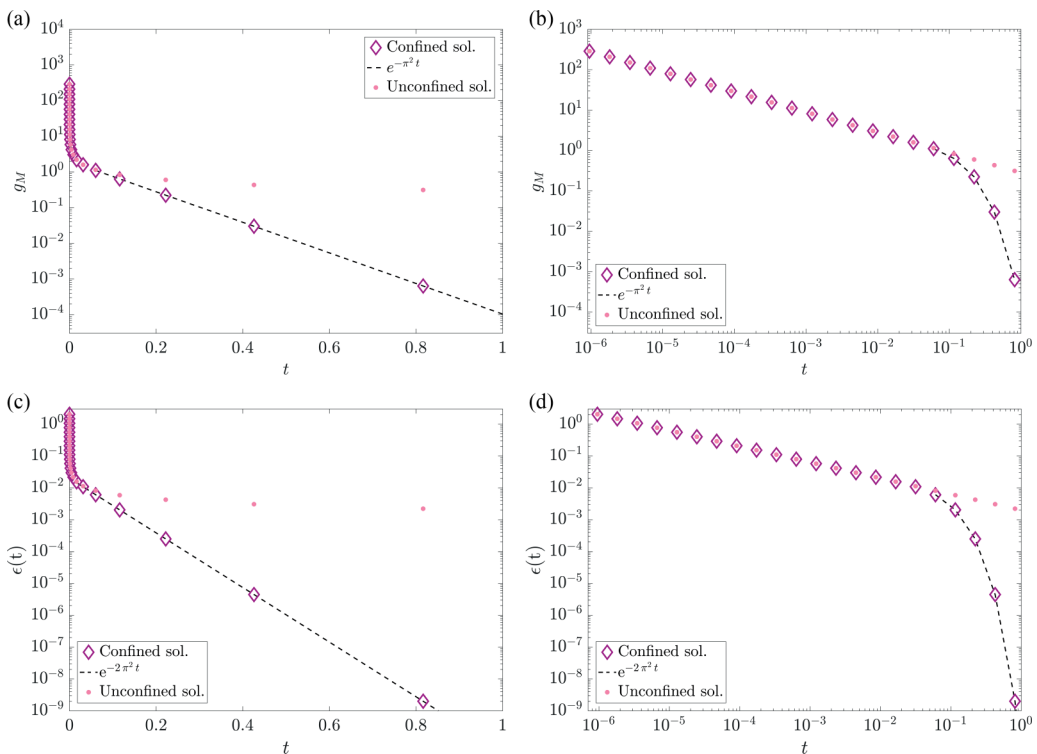


FIG. 4. Temporal evolution of the maximum gradient g_M and scalar dissipation rate ϵ for a front initial condition. The semilogarithmic plot in (a) and (c) emphasizes the exponential cutoff due to confinement that takes place around $t = 1/\pi^2$; the double-logarithmic plot in (b) and (d) emphasizes the power-law decay for early times, taking place when the confinement has no impact on diffusive mass transfer.

Eq. (18), we get

$$p_c(c) = \frac{1}{2c \sqrt{\ln(c_m/c_M) \ln(c/c_M)}}, \quad (19)$$

which is shown in Fig. 2(c). Since the solution Eq. (18) shown in Fig. 1(c) is the same as the gradient of a diffusing front, the previous expression also represents the PDF of a front gradient $p_g(g_c)$, shown in Fig. 2(b), that scales as $1/g_c$ for small values and its maximum value g_M decays with time (due to mixing), as $t^{-1/2}$.

The dilution index for an unconfined diffusing pulse is computed combining Eq. (13) with Eq. (18), to get

$$E(t) = \exp[\ln(\sqrt{4\pi t}) + 1/2] = \sqrt{4\pi t}. \quad (20)$$

The previous exact analytical expression is shown in Fig. 3(c) in a double-logarithmic plot versus time, as pink dots: from its initial value it keeps increasing at all times (slower than the initial front) as a result of the infinite space that the concentration can explore. The concentration gradient is obtained differentiating (18):

$$\nabla c(x, t) = -\frac{1}{\sqrt{4\pi t}} \frac{x - 1/2}{2t} e^{-[(x-1/2)^2/4t]}, \quad (21)$$

and it is shown in Fig. 1(d) at four time steps ($t = 0.0047, 0.013, 0.023, 0.043, \text{ and } 0.079$), as pink solid lines ranging from light to dark as time increases. Its maximum value (equal to the opposite

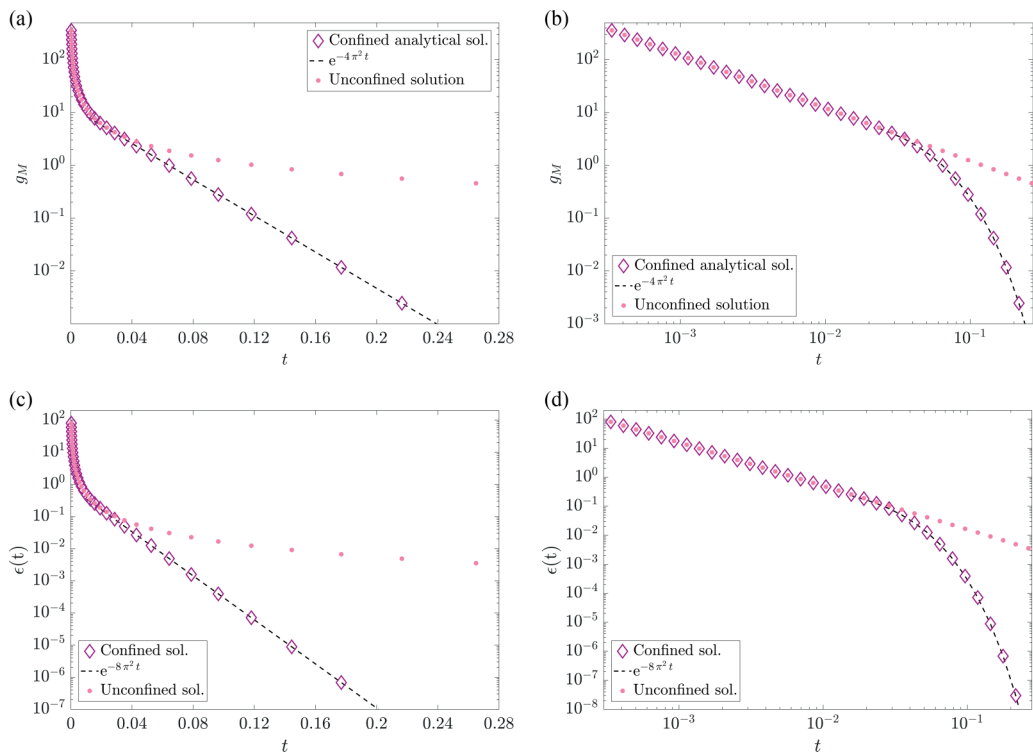


FIG. 5. Temporal evolution of the maximum gradient g_M and scalar dissipation rate ϵ for a pulse initial condition in unconfined (dots) and confined (diamonds) cases. The semilogarithmic plot in (a) and (c) emphasizes the exponential cutoff (dashed black line) due to confinement that takes place around $t = 1/\pi^2$; the double-logarithmic plot in (b) and (d) emphasizes the power-law decay for early times, taking place when the confinement has no impact on diffusive mass transfer.

of its minimum value) is reached at the moving location $x = 1/2 + \sqrt{2t}$ and its absolute value decreases with time as

$$g_M = \frac{e^{-1/2}}{\sqrt{8\pi t}}, \quad (22)$$

which is shown in Fig. 5(a) in a semilogarithmic plot and in Fig. 5(b) in a double-logarithmic plot. We cannot invert and differentiate Eq. (21) since the spatial variable x appears within the exponential argument as well as in prefactor. Thus, we compute numerically the occurrence of the values g_c from the analytical expression Eq. (21), to derive the gradient distribution $p_g(g_c)$, as a normalized histogram: the result is shown as a pink solid line in Fig. 2(d), ranging from lighter to darker as time increases, for the same steps as the profiles of Figs. 1(c) and 1(d). As for the concentration profile, the distribution of gradient values g_c scales as $1/g_c$ for small values and it increases towards its maximum value, Eq. (22).

The scalar dissipation rate defined in Eq. (16), measuring the rate of the diffusing pulse mixing, is

$$\epsilon(t) = \frac{1}{\sqrt{32\pi t^3}}, \quad (23)$$

and it is shown as pink dots in Fig. 5(c) as a semilogarithmic plot and 5(d) as a double-logarithmic plot.

Classical measures of mixing for unconfined diffusive systems are power laws of time: this implies that for these mixing phenomena a rigorous timescale cannot be defined. However, it is common to refer to $t = 1$ (in dimensional form to λ^2/D) as the characteristic diffusive timescale. We introduced it as the timescale allowing one to make the diffusion equation dimensionless; it can also be invoked from the second centered moment of a diffusing plume as the time needed for its spreading to cover the length scale of 1.

B. Confined case

Let us now consider a system where a tracer is confined within impermeable boundaries, $x \in [0, 1]$, with imposed no-flux boundary conditions. The diffusion problem is mathematically formulated as

$$\frac{\partial c}{\partial t} = \frac{\partial^2 c}{\partial x^2} \quad \text{for } x \in [0, 1] \quad \text{with } c(x, 0) = f_0(x) \quad \text{and} \quad \left. \frac{\partial c}{\partial x} \right|_{x=0,1} = 0, \quad (24)$$

with c , t , and x defined in Eq. (4). Using the method of separation of variables, we can express the problem solution as

$$c(x, t) = X(x)T(t), \quad (25)$$

which can be differentiated with respect to time and space, providing

$$\frac{\partial c}{\partial t} = X(x)T'(t) \quad \text{and} \quad \frac{\partial^2 c}{\partial x^2} = X''(x)T(t). \quad (26)$$

We then rewrite Eq. (24) as

$$X(x)T'(t) = X''(x)T(t). \quad (27)$$

Collecting time on the left-hand side and space on the right-hand side of the equation, we obtain

$$\frac{T'(t)}{T(t)} = \frac{X''(x)}{X(x)} = -\alpha, \quad (28)$$

where α is a positive constant that ensures mass conservation. We have now a system of two ordinary differential equations to be solved simultaneously:

$$X''(x) + \alpha X(x) = 0 \quad (29)$$

and

$$T'(t) + \alpha T(t) = 0. \quad (30)$$

Solving Eq. (29) for $X(x)$, we find the family of solutions $X_m(x) = A_m \cos(\sqrt{\alpha} x)$: applying the boundary condition $X'(0) = X'(1) = 0$ the only nontrivial solution is given by $\alpha = m^2 \pi^2$. Thus, Eq. (30) becomes $T'(t) = -\pi^2 m^2 T(t)$: integrating on both sides we get $T_m(t) = P_m e^{-\pi^2 m^2 t} + C$. The general solution is a linear combination of the obtained sets of solutions:

$$c(x, t) = \sum_{m=1}^{\infty} B_m \cos(\pi m x) e^{-\pi^2 m^2 t} + c_f, \quad (31)$$

with c_f the homogeneous concentration reached at $t = +\infty$ and B_m a coefficient that depends on the spatial initial distribution $f_0(x) = c(x, 0)$:

$$B_m = 2 \int_0^1 f_0(x) \cos(\pi m x) dx. \quad (32)$$

The derived solution Eq. (31) expresses the concentration profile as the superposition of modes m (functions that do not change shape as the system diffuses) that are periodic and fluctuating in space

between the domain boundaries, while temporally decaying exponentially fast with characteristic scaling $\exp(-m^2\pi^2t)$.

1. Initial concentration front

For an initial front $f_0(x) = \theta(x - 1/2)$, the profile in Eq. (31) is shown in Fig. 1 (as a pink dotted line ranging from light to dark as time increases) at the same time steps shown for the unconfined case. At early times the confined and unconfined profiles exactly overlap, while at later times they do not. On the one hand, the confined solution, due to the no-flux boundary conditions imposed, keeps a flat profile at the boundaries ($x = 0, 1$) and, thus, a steep gradient providing a strong diffusive mass flux responsible for mixing. On the other hand, the unconfined solution spreads across space smoothing its gradient, reducing dramatically the Fickian mass flux and, thus, the overall mixing.

For times larger than $t > 1/(m^2\pi^2)$ the exponential time dependence of the mode m cannot be neglected. Since for the mode $m = 1$ the coefficient $B_1 = 2/\pi$ is nonzero, it dominates the solution, Eq. (31), for times larger than $1/\pi^2$. For such times, the concentration profile is well approximated by

$$c(x, t) \approx c_f - 2/\pi \cos(\pi x)e^{-\pi^2 t}, \quad (33)$$

with the value of c that is bounded between its minimum and maximum values $c_m < c < c_M$, that are taken at the impermeable walls $x = 0, 1$ where they vary to conserve the total mass, as

$$c_m = c(x = 0, t) = c_f - 2/\pi e^{-\pi^2 t}, \quad c_M = c(x = 1, t) = c_f + 2/\pi e^{-\pi^2 t}. \quad (34)$$

At early times, $t < 1/\pi^2$, several terms of the expansion, Eq. (31), must be taken into account and we cannot invert and differentiate it to compute its PDF, $p_c(c)$. However, at such short times the solution for $c(x, t)$ is not affected by the presence of the impermeable boundaries at $x = 0$ and $x = 1$ and it is well approximated by (10), and thus also $p_c(c)$ is known and given by Eq. (12). For $t > 1/\pi^2$ we can invert and differentiate Eq. (33) to derive the probability density function. The profile is invertible on the full domain $x \in]0, 2N[$, in the confined case $N = 1/2$ so $p = 1/(2N) = 1$, and we get

$$p_c(c, t) \approx \frac{1}{2} \frac{\exp(\pi^2 t)}{\sqrt{1 - [(c_f - c)\frac{\pi}{2} \exp(\pi^2 t)]^2}}, \quad (35)$$

which is shown in Fig. 2(a) as a pink dotted line from light to dark, for increasing time. As time overcomes $1/\pi^2$ the concentration PDF becomes time dependent and it deviates from the unconfined case: for low concentrations it deviates from the scaling $\sim 1/c$ towards a U-shaped function, characterized by peaks at the smallest and largest value, Eq. (34), and it is exactly described by Eq. (35), as shown in Fig. 2(a) (diamonds).

We were not able to derive an analytical expression for the dilution index for this case and, thus, it has been computed numerically inserting Eq. (31) within the definition of E , Eq. (13). This is shown in Fig. 3(a) where the confined case from its initial value $E(t = 0) = 1$ rises up to its final plateau for times larger than $t > 1/\pi^2$ corresponding to

$$E(t) = \exp \left[- \int c_f \ln(c_f) dx \right] = \exp[-1/2 \ln(1/2)] = \sqrt{2}, \quad (36)$$

implying that the macroscopic mixing state of the diffusing system stops evolving, while the unconfined case grows indefinitely. Moreover, the semilogarithmic plot of E versus \sqrt{t} shown in Fig. 3(b) highlights the higher degree of mixing of the confined case for times even shorter than $\sqrt{0.1}$ corresponding to times shorter than 0.01.

For large times, $t > 1/\pi^2$, we compute the gradient of Eq. (33):

$$\nabla c \approx 2 \sin(\pi x)e^{-\pi^2 t}. \quad (37)$$

The above expression for ∇c , whose value we denote by g_c , can be inverted and differentiated to compute its probability density function as

$$p_g(g_c) \approx \frac{1}{2\pi} \frac{\exp(\pi^2 t)}{\sqrt{1 - [\frac{1}{2}g_c \exp(\pi^2 t)]^2}}, \quad (38)$$

shown in Fig. 2(b) (diamonds). We remark that for a front initial condition the concentration is dissipated very quickly and the values c_m and c_M approach exponentially fast the asymptotic value c_f , flattening the spatial profile: this is reflected on the concentration PDF $p_c(c)$ that deviates from the unconfined $1/c$ to become flat at low c values where it gets the value $\beta \approx \frac{\exp(4\pi^2 t)}{4\pi}$, as shown in Fig. 2(b) and its inset. The concentration gradient reaches its maximum value, g_M , at location $x = 1/2$:

$$g_M = \nabla c(x = 1/2, t) = 2e^{-\pi^2 t}, \quad (39)$$

and decays much faster (exponentially fast) than the power-law decrease of the unconfined case, as shown in Figs. 4(a) and 4(b). This change in temporal decay is due to the fact that to conserve mass the concentration value at the boundaries vary exponentially fast [see Eq. (34)] as the tracer gets accumulated there due to the spatial confinement.

From the spatial profile of the concentration gradient Eq. (37), we compute the analytical expression of the scalar dissipation rate for $t > 1/\pi^2$ as

$$\epsilon(t) \approx 2e^{-2\pi^2 t}, \quad (40)$$

whose exponential decay, shown in Figs. 4(c) and 4(d) superposed to the slower power-law decay $1/\sqrt{8\pi t}$ of the unconfined case, has the characteristic time $1/(2\pi^2)$.

2. Initial pulse

We now consider an initial pulse $f_0(x) = \delta(x - 1/2)$. Since $B_1 = 0$, for times larger than $1/(4\pi^2)$, the leading mode of Eq. (31) is $m = 2$ (and $B_2 = -2$) so that

$$c(x, t) \approx c_f - 2 \cos(2\pi x) \exp(-4\pi^2 t), \quad (41)$$

with the concentration value bounded between its minimum and maximum values c_m and c_M , respectively, which are

$$c_m = c(0, t) = c_f - 2e^{-4\pi^2 t}, \quad c_M = c(1/2, t) = c_f + 2e^{-4\pi^2 t}. \quad (42)$$

We observe that, unlike in the unconfined case, the concentration profile for the pulse initial condition differs from the gradient of a diffusing front. The former decays exponentially with a characteristic time which is four times shorter: $1/(4\pi^2)$ instead of $1/\pi^2$. Moreover, the two spatial profiles are different since the front gradient is zero at the boundaries ($x = 0$ and $x = 1$) to ensure no flux at impermeable walls, while the pulse solution, to conserve the mass, is always above zero and it increases at both boundaries with time.

For early times $t < 1/(4\pi^2)$ several terms of the sum in (31) must be taken into account and we cannot invert it to compute $p_c(c)$. However, at such short times the solution for c is not affected by the presence of the impermeable boundaries at $x = 0$ and $x = 1$ and it is well approximated by (18) and thus also $p_c(c)$ is known. At large times, we invert and differentiate the concentration spatial profile Eq. (41) on half of the domain, $x \in]0, N[$ so $p = 1/N = 2$, to derive the probability density function $p_c(c)$ as

$$p_c(c, t) \approx \frac{\exp(4\pi^2 t)}{2\pi \sqrt{1 - \left(\frac{(c-c_f)\exp(4\pi^2 t)}{2}\right)^2}}, \quad (43)$$

shown in Fig. 2(c) (diamonds). We remark that for a pulse initial condition the concentration is dissipated very quickly and the values c_m and c_M approach exponentially fast the asymptotic value c_f , flattening the spatial profile: this is reflected on the concentration PDF $p_c(c, t)$ that deviates from the scaling $1/c$ towards a U shape.

As for the front case, we were not able to derive an analytical expression for the dilution index in a confined domain, thus, it has been computed numerically inserting Eq. (31) within the definition of E , Eq. (13). This is shown in Fig. 3(c) where the confined case deviates from the unconfined one at times even shorter than $1/(2\pi^2)$ to reach its final plateau. This shorter mixing time can be understood analyzing the scalar dissipation rate, discussed below.

We compute the corresponding concentration gradient considering only the dominant term $m = 2$, and we have

$$\nabla c(x, t) \approx 4\pi \sin(2\pi x) e^{-4\pi^2 t}. \quad (44)$$

The above expression for the concentration gradient, whose value is denoted by g_c , can be inverted and differentiated to compute its probability density function as

$$p_g(g_c) \approx \frac{\exp(4\pi^2 t)}{8\pi^2 \sqrt{1 - \left[\frac{1}{4\pi} g_c \exp(4\pi^2 t)\right]^2}}, \quad (45)$$

where its minimum and maximum values are reached at the steady locations $x = 1/4$ and $x = 3/4$, respectively:

$$g_m = \nabla c(x = 1/4, t) = 4\pi e^{-4\pi^2 t} \quad \text{and} \quad g_M = \nabla c(x = 3/4, t) = -4\pi e^{-4\pi^2 t}. \quad (46)$$

Note that for the unconfined case the locations where $\nabla c = g_m, g_M$ are moving as \sqrt{t} away from x_0 . As for the concentration, also the gradient profile flattens at large times and its PDF $p_g(g_c)$ deviates from the unconfined $1/c$ scaling to become constant at low c values where it gets the value $\beta \approx \frac{\exp(4\pi^2 t)}{8\pi^2}$, as shown in Fig. 2(d) and its inset. From the spatial profile Eq. (44), we compute the scalar dissipation rate as

$$\epsilon(t) \approx 8\pi^2 e^{-8\pi^2 t}, \quad (47)$$

which is shown in Figs. 5(c) and 5(d) in a semilogarithmic and double-logarithmic plot, respectively, to highlight its exponential decay which is much faster than the power-law scaling of the unconfined case. We note that the exponential decay characteristic time is $1/(8\pi^2)$ and it is shorter than the $1/(2\pi^2)$ characteristic of mixing for the front case, as observed also in the dilution index analysis, discussed above.

3. Numerical solutions as control

We tested all our analytical derivations against numerical solutions of the diffusion equation in a confined domain. We adopted a backward finite difference simulation scheme for the diffusion equation in a one-dimensional and confined domain, with no-flow boundary condition. The initial conditions we impose to the front and pulse initial conditions are defined as Eqs. (10) and (18) for $t = t_0 = 10^{-8}$, respectively, which corresponds to the two theoretical initial configurations that underwent a little diffusion. The numerical results show that our derived solutions accurately describe the physical problem (the mean-squared error between the two profiles is below $10^{-8} c_0$ at all times). All expressions we derived for concentration profiles and mixing measures are in excellent agreement with the numerical simulations.

III. IMPACT

We showed that diffusion in a confined domain is qualitatively and quantitatively different from diffusion in an unconfined and continuous domain. To illustrate the potential impact of the discussed

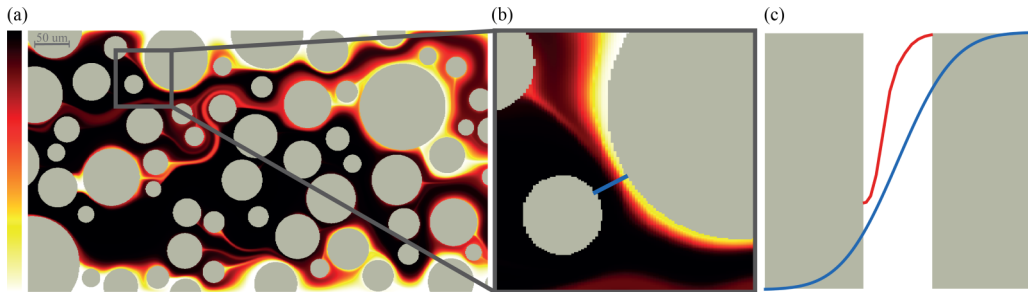


FIG. 6. (a) Concentration field in a porous medium composed of round grains (gray disks) for $Pe = 2500$ after rescaled time $t/\tau_A = 40$. (b) Zoom-in of the same concentration field in a pore. (c) The blue line shows a diffusive unconfined concentration profile; the red line represents the interpolated concentration profile along the blue segment in (b).

results on mixing within confined media, we simulate, as a proof of concept, the displacement of a mixing front in a porous material. We run a numerical simulation for Stokes flow in a $1 \text{ mm} \times 3 \text{ mm}$ porous medium with a prescribed geometry, no-slip boundary conditions at grains walls (gray disks in Fig. 6), characterized by an average pore throat size of $l = 0.05 \text{ mm}$, resulting in an average fluid velocity of 1 mm/s (Reynolds number $Re = lu/v = 0.05$). In this flow we solve the transport of a passive solute Eq. (1) continuously injected from the left-hand side of the system, with no-flux boundary conditions at the grain walls. A snapshot of the concentration field transported within a porous medium for a Péclet number $Pe = \tau_D/\tau_A = ul/D = 2500$ (a measure of the relative importance of advective and diffusive mechanisms) is given in Fig. 6(a) after 40 advective time steps ($t = 40t_A$). For the $Pe = 2500$, this corresponds to $\approx 1.5\%$ of the diffusive time, which would imply a very sharp front where diffusion has not had the time to play a role at the scale of a pore. Instead, the figure shows that diffusion had the time to smear the pore-scale concentration gradients within the pores. This would be consistent with the much smaller $Pe = t_\epsilon/\tau_A = 250$, defined with respect to the confinement-limited diffusion timescale t_ϵ , defined in terms of the scalar dissipation rate, for which 40 advective timescales correspond to $\approx 15\%$ of it.

The concentration field is heterogeneously distributed across the pores and along the fluid displacement front, which is stretched and elongated resulting in a lamellar structure. In Fig. 6(b) we show a zoom-in view of mixing at a single pore throat, to highlight the pore scale nonmixed condition, which is quantified in Fig. 6(c) where the interpolation of the concentration field across the pore throat is shown in red. We observe that the concentration profile confined in a pore is qualitatively different from its unconfined counterpart (blue line); indeed the presence of an impermeable boundary (i) prevents the solute from diffusing freely, (ii) enhances the diffusive flux decreasing the scalar dissipation rate, (iii) resulting in a rise of the small concentration values [left-hand side of the red line in Fig. 6(c)]. This example qualitatively illustrates the potential impact of the impermeable boundary conditions on mixing state and rate in confined environments. To properly capture the mixing dynamics taking place in these porous systems, the derived confined solution for diffusion must be incorporated with the stretching dynamics in a lamellar framework, where the distribution of the confinement length scale l and the stretching of the front associated to the host medium heterogeneity are coupled in a nontrivial way. A detailed study of mixing in such a complex and confined flow system goes beyond the research presented in this article, but must incorporate the results presented here for diffusion alone.

IV. CONCLUSIONS

Diffusion is the key mixing mechanism in fluid systems, since it ultimately homogenizes concentrations, also in the presence of stretching and compression by velocity heterogeneity. We present

analytical results of the one-dimensional diffusion equation in a confined domain, characterized by the presence of no flux boundaries, separated by a distance λ , that prevent the solute concentration from diffusing freely and explore wider areas of space. We show how diffusion is affected by the confined nature of the considered spatial domain and we quantify its impact on mixing.

The general solution of the diffusion equation in a confined domain, Eq. (31), expresses the concentration profile of a diffusive tracer as the superposition modes m (functions that do not change shape as the system diffuses) that are periodic and fluctuating in space between the domain boundaries, and temporally decaying exponentially fast, scaling as $\exp(-m^2\pi^2t)$. As far as the diffusing tracer does not experience the presence of the impermeable boundaries [e.g., right after the injection of a pulse in the middle of the domain $t < 1/(m^2\pi^2)$] the exponential decay of the modes is not substantially changing their amplitude and a large number of modes must be taken into account to describe the tracer concentration profile, recovering the solution of the unconfined case. In such conditions space and time are coupled and the concentration profile can be expressed in terms of the classical dimensionless coordinate for diffusion, $\xi = x/\sqrt{2Dt}$, making the profile self-similar and scale independent, which is reflected in the slow, power-law decay of several mixing measures. However, as soon as a single mode m dominates the sum, space and time are decoupled and the exponential decay of the solution defines a characteristic timescale [$1/(m^2\pi^2)$], as reflected by the exponential decay of the mixing measures considered.

Physically, in a confined space the no-flux boundary condition $\nabla c(0, t) = \nabla c(\lambda, t) = 0$ imposes a flat profile at the domain edges leading to an overall steeper gradient and higher mass flux compared to the unconfined case where mass can freely diffuse exploring wide areas of space, slowly dissipating the concentration gradients. Therefore local and global measures of mixing display significantly different dynamics. We show that, maximum concentration gradients and scalar dissipation rate drop exponentially fast and the dilution index E reaches a plateau, while they typically follow a slower power-law decrease in an unconfined domain and E grows indefinitely. Also the concentration and gradient distribution (PDF) significantly change their shape and dynamics. This exponential time scaling of mixing measures in confined conditions leads to the definition of a new characteristic timescale for diffusion, which depends on the initial condition, and it is fixed by the leading mode (e.g., $m = 1$ for a front and $m = 2$ for a pulse), $\lambda^2/(m^2D\pi^2)$, which is much shorter (one order of magnitude shorter) than the characteristic λ^2/D defined to rescale the diffusion equation.

These observations show that the homogenization dynamics (mixing) is significantly faster under confinement, i.e., no-flux boundary conditions. In more complex scenarios, where the host medium heterogeneity must be taken into account, diffusion must be coupled with flow and fluid stretching variability [1,8] as well as confinement scale λ that can change considerably [20]. For example, in a lamellar framework [8,21], the local confinement scale λ should be normalized by the lamella width $s(t)$ and time is rescaled by the characteristic diffusive time over a lamella width $\bar{t} = D \int_0^t 1/s(t')^2 dt'$, since fluid stretching affects the local diffusion process by keeping the gradients steep. In such scenario, the boundary conditions become space and time dependent and given by

$$\left. \frac{\partial c}{\partial \bar{n}} \right|_{\bar{n}=0, \lambda/s(\bar{t})} = 0. \quad (48)$$

Furthermore, in a heterogeneous medium λ must be defined locally, leading to a space-dependent characteristic timescale. Implementing a full mixing model taking into account no-flux boundary conditions at domain boundaries is nontrivial and requires further work. However, neglecting confinement-limited diffusion to describe mass transport phenomena may lead to an incorrect description of mixing.

ACKNOWLEDGMENTS

The research leading to these results has received funding from the Swiss National Science Foundation, Project No. 200021_172587, ‘‘Flows in confined micro-structures: Coupling physical heterogeneity and bio-chemical processes.’’

- [1] E. Villermaux, Mixing versus stirring, *Annu. Rev. Fluid Mech.* **51**, 245 (2019).
- [2] J. Happel and H. Brenner, *Low Reynolds Number Hydrodynamics* (Martinus Nijhoff Publishers, Leiden, 1983).
- [3] J. Ottino, *The Kinematics of Mixing: Stretching, Chaos, and Transport* (Cambridge University Press, Cambridge, UK, 1989).
- [4] E. Villermaux and J. Duplat, Mixing is an aggregation process, *C. R. Mécanique* **331**, 515 (2003).
- [5] J. J. Hidalgo, J. Fe, L. Cueto-Felgueroso, and R. Juanes, Scaling of Convective Mixing in Porous Media, *Phys. Rev. Lett.* **109**, 264503 (2012).
- [6] B. Jha, L. Cueto-Felgueroso, and R. Juanes, Synergetic Fluid Mixing from Viscous Fingering and Alternating Injection, *Phys. Rev. Lett.* **111**, 144501 (2013).
- [7] P. K. Kitaniadis, The concept of the dilution index, *Water Resour. Res.* **30**, 2011 (1994).
- [8] T. Borgne Le, M. Dentz, and E. Villermaux, The lamellar description of mixing in porous media, *J. Fluid Mech.* **770**, 458 (2015).
- [9] S. Pope, *Turbulent Flows* (Cambridge University Press, New York, 2000).
- [10] S. Whitaker, *The Method of Volume Averaging* (Springer, New York, 1999).
- [11] M. Dentz, T. Le Borgne, A. Englert, and B. Bijeljic, Mixing, spreading and reaction in heterogeneous media: A brief review, *J. Contam. Hydrol.* **120-121**, 1 (2011).
- [12] E. Villermaux and C. Innocenti, On the geometry of turbulent mixing, *J. Fluid Mech.* **393**, 123 (1999).
- [13] P. de Anna, J. Jimenez-Martinez, H. Tabuteau, R. Turuban, T. L. Borgne, M. Derrien, and Y. Meheust, Mixing and reaction kinetics in porous media: An experimental pore scale quantification, *Environ. Sci. Technol.* **48**, 508 (2014).
- [14] P. de Anna, M. Dentz, A. Tartakovsky, and T. Le Borgne, The role of filament dynamics in reaction front kinetics, *Geophys. Res. Lett.* **41**, 4586 (2014).
- [15] W. Ranz, Applications of a stretch model to mixing, diffusion, and reaction in laminar and turbulent flows, *AIChE J.* **25**, 41 (1979).
- [16] P. Meunier and E. Villermaux, The diffusive strip method for scalar mixing in two dimensions, *J. Fluid Mech.* **662**, 134 (2010).
- [17] R. Rusconi, M. Garren, and R. Stocker, Microfluidics expanding the frontiers of microbial ecology, *Annu. Rev. Biophys.* **43**, 65 (2014).
- [18] P. de Anna, A. A. Pahlavan, Y. Yawata, R. Stocker, and R. Juanes, Chemotaxis under flow disorder shapes microbial dispersion in porous media, *Nat. Phys.* (2020), doi:10.1038/s41567-020-1002-x.
- [19] A. Fick, Über diffusion, *Ann. Phys.* **170**, 59 (1855).
- [20] P. de Anna, B. Quaife, G. Biroso, and R. Juanes, Prediction of the low-velocity distribution from the pore structure in simple porous media, *Phys. Rev. Fluids* **2**, 124103 (2017).
- [21] T. Le Borgne, M. Dentz, and E. Villermaux, Stretching, Coalescence and Mixing in Porous Media, *Phys. Rev. Lett.* **110**, 204501 (2013).